Multi-Electron Transfer at H-Terminated p-Si Electrolyte Interfaces: Large Photovoltages under Inversion Conditions

Multi-Electron Transfer at H-terminated p-Si Electrolyte Interfaces: Large Photovoltages under Inversion Conditions

Niklas D. Keller,[1] Pierpaolo Vecchi,[1,2] David C. Grills,[3] Dmitry E. Polyansky,[3] Gabriella P. Bein,[1] Jillian L. Dempsey,[1] James F. Cahoon,[1] Gregory N. Parsons,[4] Renato N. Sampaio,[1]* and Gerald J. Meyer[1]*

[1]Department of Chemistry, University of North Carolina at Chapel Hill, Chapel Hill, NC 27599
[2]Department of Physics and Astronomy, University of Bologna, Bologna, Italy 40127
[3]Chemistry Division, Brookhaven National Laboratory, Upton, NY 11973-5000
[4]Department of Chemical and Biomolecular Engineering, North Carolina State University, Raleigh, North Carolina 27695-7905

Abstract

Photovoltages for hydrogen terminated p-Si(111) in an acetonitrile electrolyte were quantified with methyl viologen [1,1'-$(CH_3)_2$-4,4'-bipyridinium]$(PF_6)_2$, abbreviated MV^{2+}, and $[Ru(bpy)_3](PF_6)_2$, where bpy is 2,2′-bipyridine, that respectively undergo two and three one-electron transfer reductions. The reduction potentials, $E°$, of the two MV^{2+} reductions occurred at energies within the forbidden bandgap, while the three $[Ru(bpy)_3]^{2+}$ reductions occurred within the continuum of conduction band states. Bandgap illumination resulted in reduction that were more positive than that measured with a degenerately doped n^+-Si demonstrative of a photovoltage, V_{ph}, that increased in the order: $MV^{2+/+}$ (260 mV) < $MV^{+/0}$ (400 mV) < $Ru^{2+/+}$ (530 mV) ~ $Ru^{+/0}$ (540 mV) ~ $Ru^{0/-}$ (550 mV). Pulsed 532 nm excitation generated electron-hole pairs whose dynamics were nearly constant under depletion conditions and increased markedly as the potential was raised or lowered. A long wavelength absorption feature assigned to conduction band electrons provided additional evidence for the presence of an inversion layer. Collectively, the data reveal that the most optimal photovoltage, as well at the longest electron-hole pair lifetime and the highest surface electron concentration, occur when $E°$ lies energetically within the unfilled conduction band states where an inversion layer is present. The bell-shaped dependence for electron-hole pair recombination with the surface potential was predicted by the time-honored SRH model providing a clear indication that this interface provides access to all four bias conditions, i.e., accumulation, flat band, depletion, and inversion. The implications of these findings for photocatalysis applications and solar energy conversion are discussed.

*Renato N. Sampaio renatons@email.unc.edu
Gerald J. Meyer gjmeyer@email.unc.edu

Introduction

Hybrid photoelectrodes comprised of a narrow bandgap semiconductor with an integrated molecular catalyst are actively being investigated for the generation of fuels from chemical feedstocks and sunlight.[1-11] The interfacial electron transfer processes that govern the efficiency of such hybrids are understood through a model that requires isoenergetic transfer between the catalyst and photogenerated carriers at the fixed energetic position of the conduction or valence band edge.[12-15] This model was first described in the 60s by the combined theoretical work of Marcus and Gerischer,[12-13] and continue to be disseminated in modern research publications and text books of electron transfer theories.[14-15] This energetic requirement is suitable for optimization of single electron transfers of importance to regenerative solar cells,[16] yet remains challenging for important multi-electron catalysis such as water oxidation and carbon dioxide reduction. Herein, we report electron transfer, photovoltage, and kinetic behavior of illuminated p-Si electrolyte interfaces in contact with redox active species that accept multiple electrons.

To appreciate challenges associated with multi-electron transfer photocatalysis at a semiconductor-electrolyte interface, consider the hypothetical electrostatic potential alignment shown in Scheme 1, where the energetic positions of the conduction band edge (V_{CB}) and reduction potentials (E^{o}) of a molecular catalyst are rigidly fixed relative to one another. Consider further a generic catalytic cycle comprised of a resting state, Cat, that undergoes two sequential one-electron transfers for the net two-electron catalytic reduction of CO_2 to CO.[1] In this hypothetical representation, the first reduction potential, $E°(Cat^{n/n-1})$, is within the forbidden bandgap of the semiconductor and energetically closer to the semiconductor Fermi level, V_F, than is $E°(Cat^{n-1/n-2})$. Upon equilibration, interfacial charge transfer occurs until V_F aligns with $E°(Cat^{n/n-1})$. Due to the low density of carriers in the semiconductor, essentially all of the potential drop occurs in the semiconductor, as depicted by the band bending in Scheme 1. The energetic position of V_{CB} relative to $E°(Cat^{n/n-1})$ at the semiconductor-electrolyte is unchanged. Activationless isoenergetic transfer is expected when V_{CB} lies energetically above $E°$ by a magnitude equal to the reorganization energy.[12-13]

Transfer of the second electron is energetically unfavored for an electron at V_{CB} as shown in Scheme 1. Transfer from a non-thermalized electron is possible,[17] but prior research has shown that such "hot" interfacial electron transfer is highly inefficient due to strong electron-phonon interactions.[15, 18-21] Instead, efficient electron transfer would require a semiconductor with a more negative V_{CB} (closer to the vacuum level). Even if an alternative semiconductor material was identified for the second reduction, this material would necessarily have band edge positions less favorable for the first reduction. Hence, optimization of single electron transfers at semiconductor-electrolyte interfaces may be achieved through energetic alignment,[16, 22] but the requirements of

fixed band edge positions present significant challenges for optimization of multi-electron transfer catalysis.

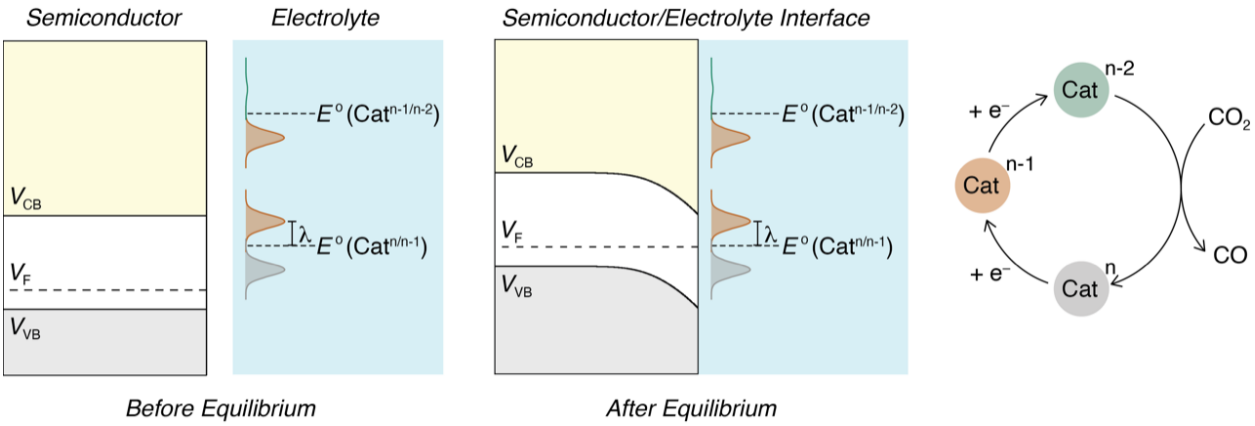

Scheme 1. Hypothetical interfacial energetics at a semiconductor electrolyte interface for a generic catalytic two-electron reduction of CO_2 to CO. Before equilibrium, $E^o(Cat^{n/n-1})$ lies within the forbidden bandgap while $E^o(Cat^{n-1/n-2})$ is within the continuum of unfilled conduction band states. At equilibrium, the Fermi energy (V_F) is equal to $E^o(Cat^{n/n-1})$ and a depletion layer shown by band bending serves to sweep conduction band electrons toward the catalyst and valence band holes toward the semiconductor bulk. With a model where the band edge positions are fixed, the first reduction in the catalytic cycle is ideal and would generate the largest photovoltage. In contrast, the second reduction – with $E^o(Cat^{n-1/n-2})$ above the conduction band edge, V_{CB} – is expected to be highly inefficient.

The energetic alignment shown for the first reduction in Scheme 1 is most optimal for interfacial electron transfer *and* for generation of a large photovoltage.[13, 23-24] In contrast, electron transfer is not expected to be efficient for the second reduction because the potential falls outside the forbidden bandgap.[23] This is important as the photovoltage is the maximum Gibbs free energy available from bandgap excitation. Herein, the assumption of fixed band edge positions is shown to be incorrect for multi-electron transfer at H-terminated p-Si electrolyte interfaces. The largest photovoltage was indeed realized when the E^o is within the continuum of conduction band states, like that shown for $E^o(Cat^{n/n-1})$

In 1986 researchers at Bell Labs reported that a hydrofluoric acid etch of a Si(111) crystal provided a surface that was remarkably inactive from an electronic point of view – by removal, or passivation, of surface states.[25] Infrared spectroscopy revealed that the surface was terminated with Si-H bonds that were stable in air for minutes.[26] The H-termination maintained the tetrahedral coordination of the Si atoms and removed the 'dangling bonds' that serve as recombination centers for photogenerated electron-hole pairs.[26-27] Indeed, the surface recombination velocity reported in this seminal work was the lowest ever measured.[25] A review of the photoelectrochemical literature reveals that such ideal electronic interfaces have received surprisingly little attention for multi-

electron transfer catalysis even though they have enabled high efficiencies in regenerative solar cells based on one-electron redox mediators.[16, 22]

Here we report the photoelectrochemical behavior of H-terminated p-Si in acetonitrile electrolytes with two molecular species that accept multiple electrons by sequential outer-sphere transfers: methyl viologen [1,1'-$(CH_3)_2$-4,4'-bipyridinium]$(PF_6)_2$, abbreviated MV^{2+}, which undergoes two sequential one-electron transfers; and ruthenium tris-bipyridyl $[Ru(bpy)_3]^{2+}$ which undergoes three sequential reductions ($Ru^{2+/+}$, $Ru^{+/0}$, $Ru^{0/-}$). Importantly, the $E°$ values span a range greater than the 1.12 eV band gap of Si, enabling a test of the assumption of fixed band edge positions for interfacial electron transfer. Electrochemical measurements indicate that all three $[Ru(bpy)_3]^{2+}$ reduction potentials lie energetically within the continuum of unfilled conduction band states while the two MV^{2+} reductions reside within the forbidden bandgap. Time-resolved and steady-state infrared spectroscopy are introduced as new tools for the characterization of photoelectrochemical cells that provides compelling evidence for a transition from the depletion condition to an inversion layer as the Fermi level is raised above the conduction band edge, toward the vacuum level. Kinetic evidence for an accumulation layer at more positive potentials indicates that the H-terminated p-Si acetonitrile electrolyte interface provides access to all four bias conditions known for semiconductor interfaces in the solid state, i.e., accumulation, flat band, depletion, and inversion. The bell-shaped dependence of the surface recombination rate on the surface potential, quantified herein by nanosecond time-resolved infrared spectroscopy, validates a statistical SRH theory reported over 60 years ago.[15, 28-33] An important conclusion from this research is that the most optimal photovoltage and surface electron concentration for multi-electron transfer catalysis occur when the acceptor $E°$ value lies above the conduction band edge and not within the bandgap as is normally assumed.[13, 24]

Experimental

General considerations

Acetonitrile (CH_3CN, spectrochemical grade, Burdick and Jackson, Honeywell) was deoxygenated with N_2 and transferred into a N_2 atmosphere glovebox for further use. Buffered oxide etchant (BOE, 10:1, Sigma-Aldrich), gallium-indium eutectic (GaIn eutectic, Ga 75.5% / In 24.5%, ≥ 99.99% trace metals basis, Sigma-Aldrich) were used as received. Ferrocene (Fc, CAS: 3109-63-5, 98%, Sigma-Aldrich) was purified by sublimation prior to use. Tetrabutylammonium hexafluorophosphate ($TBAPF_6$, CAS: 3109-63-5, for electrochemical analysis, ≥99%, Fluka) was recrystallized 3 times prior to use. $[Ru(bpy)_3](PF_6)_2$ and $[MV](PF_6)_2$ (MV^{2+} is methyl viologen) were synthesized by metathesis of commercially available $[Ru(bpy)_3](Cl)_2$ (CAS 50525-27-5, Sigma Aldrich 99.95%) and $MV(Cl)_2$ (CAS 75365-73-0, Sigma Aldrich 98%). $[MV](PF_6)_2$ was recrystallized to yield white needle crystals. Boron-doped p-type silicon wafers (P/B <111> off 4º,

1 – 20 Ω cm, 380 ± 25 μm, single-side polished for cyclic voltammograms, and double polished for time-resolved infrared measurements were purchased from NOVA Electronic Materials (TX, USA). Unless otherwise noted, all measurements were performed at room temperature in nitrogen saturated CH_3CN with 0.1 M $TBAPF_6$ as the supporting electrolyte.

Silicon Photoelectrode Preparation

The silicon crystals were diced into 1.5 × 1.5 cm squares for photoelectrochemical studies and in 2.0 × 2.0 cm squares for infrared studies. The crystals were cleaned for 30 min in a piranha etch (3:1 H_2SO_4/H_2O_2; use with caution), rinsed with H_2O and dried under a stream of N_2. The slides were then HF etched for 40 s using a buffered oxide etchant (10:1) with >5% HF, washed with water, acetone and then dried under a N_2 stream. Ohmic contacts were made by scratching the unpolished side of the p-Si slides with a diamond-tipped scribe and removing the fine particles with an argon stream; GaIn eutectic was then rubbed onto the scratched area with a plastic spatula and covered with conductive Cu tape. The prepared silicon photoelectrodes were then brought into an inert N_2 atmosphere glovebox for the final preparations and measurements.

(Photo-)Electrochemistry

All (photo-)electrochemical experiments were performed using a home-built photoelectrochemical cell, with a CH Instrument potentiostat workstation (model CHI 760E) in a three-electrode configuration, inside an inert N_2 atmosphere glovebox. The working electrode was either p-Si or glassy carbon (GC), and a Pt mesh was used as the counter electrode. A leakless Ag/AgCl electrode (eDAQ, ET072-1) was used as the reference electrode and referenced to the ferrocenium/ferrocene ($Fc^{+/0}$) redox couple before and after each experiment. All reduction potentials and interfacial energetics herein are reported vs $Fc^{+/0}$. For voltammograms of illuminated p-Si, a red (650 nm) LED (Lumencor, SPECTRA 7-LCR-XA) was employed with a maximum irradiance of 34 mW cm^{-2}.

Infrared Spectroelectrochemistry and Time-Resolved Spectroscopy

Double-polished silicon photoelectrodes were used with a home-built spectroelectrochemical cell for transmission experiments in the infrared region, Figure 1. Ohmic contacts were made by scratching a ring area on one of the sides of the double-side polished Si wafer with a diamond-tipped scribe and removing the fine particles with an argon stream; GaIn eutectic was then rubbed onto the scratched area with a plastic spatula and covered with a ring of conductive Cu tape. The gas-tight cell was filled with electrolyte solution directly from an N_2 filled glovebox. Spectroelectrochemical measurements were performed with a Bruker VERTEX 80v Fourier-transformed infrared (FTIR) spectrometer. Time-resolved infrared (TRIR) measurements were performed with a benchtop nanosecond transient mid-IR spectrometer (inspIRe, Magnitude Instruments) equipped with pulsed 532 nm excitation laser and a germanium bandpass filter (1 – 5 μm). Fixed applied potentials were controlled by a CH Instrument electrochemical workstation

model CHI 760E using a Pt mesh as the counter electrode and a leakless Ag/AgCl reference electrode. All applied potentials were referenced to $Fc^{+/0}$. Additional quantum cascade laser-based time-resolved infrared measurements with various pulsed laser excitation energies (410, 500, 600 and 700 nm) were conducted with an experimental setup in the Artificial Photosynthesis group at Brookhaven National Laboratory.[34-35]

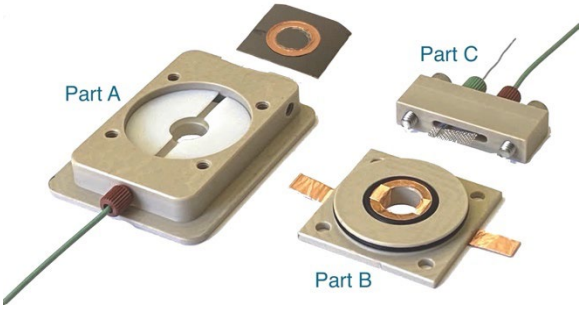

Figure 1. The gas-tight photoelectrochemical cell used for spectroelectrochemical IR measurements. A calcium fluoride (CaF_2) window is placed at the main body of the cell (part A), followed by a Teflon spacer that determines the optical pathway through the electrolyte solution. The Si wafer was placed on top of the Teflon spacer and serves as both the working electrode and the second optical window. Part B, a complementary ring of Cu foil, and the Si wafer were pressed together and tightened onto Part A with four screws. Part C hosts the Pt mesh counter electrode that was positioned at the upper part of Part A. A custom made leakless Ag/AgCl electrode (eDAQ, 1 mm thick) is used as the reference electrode. The electrolyte solution was introduced into the cell from using a gas-tight syringe or directly from an inert glovebox with PEEK tubing.

Electrochemical Impedance Spectroscopy and Mott-Schottky Analysis

The flatband potential V_{fb} and the acceptor density N_a of the H-terminated Si photocathodes in 0.1 M $TBAPF_6$ acetonitrile solution were estimated from Mott-Schottky analysis of potential-dependent capacitance data. The applied potential was scanned between −0.3 and −1.2 V vs $Fc^{+/0}$ with a step size of 10 mV. The capacitance C was extracted by modelling the impedance response of the photocathode with a single RC parallel circuit over a range of frequencies greater than 300 Hz.

Results

Cyclic voltammograms of an CH_3CN solution containing stoichiometric concentrations (1 mM) of methyl viologen (MV^{2+}) and ruthenium tris-bipyridyl $[Ru(bpy)_3]^{2+}$ with 100 mM $TBAPF_6$ electrolyte are shown in Figure 2a. Voltammograms were measured in the dark with a degenerately doped n^+-Si electrode as well as with a glassy carbon electrode (data not shown, but results were identical to those shown for n^+-Si), and with an illuminated (λ_{ex} = 650 nm, 34 mW cm^{-2}) p-Si

photoelectrode; no waves were observed over this potential window in the absence of band gap illumination. The data show two sequential MV^{2+} waves and three sequential $[Ru(bpy)_3]^{2+}$ waves. The half-wave potentials, $E_{1/2}$, as an approximation for the reduction potentials, $E°$, were in good agreement with previous reports.[23] The voltammograms were stable and could be measured over periods of hours without significant change, consistent with a previous report.[1] The half-wave potentials, $E_{1/2}$, were much less negative at the illuminated p-Si electrodef(E) than those measured with a GC electrode or a degenerately doped n^+-Si electrode ($E°$). This was also true for cobaltocene ($CoCp_2$) that was measured independently. The photovoltage, V_{ph}, defined as the difference in the measured reduction potentials for the illuminated p-Si relative to the dark n^+-Si, i.e., $V_{ph} = E_{1/2}(\text{p-Si}) - E_{1/2}(n^+\text{-Si})$, determined for at least eight separate measurements on eight different samples are given in Figure 2b and Table 1.

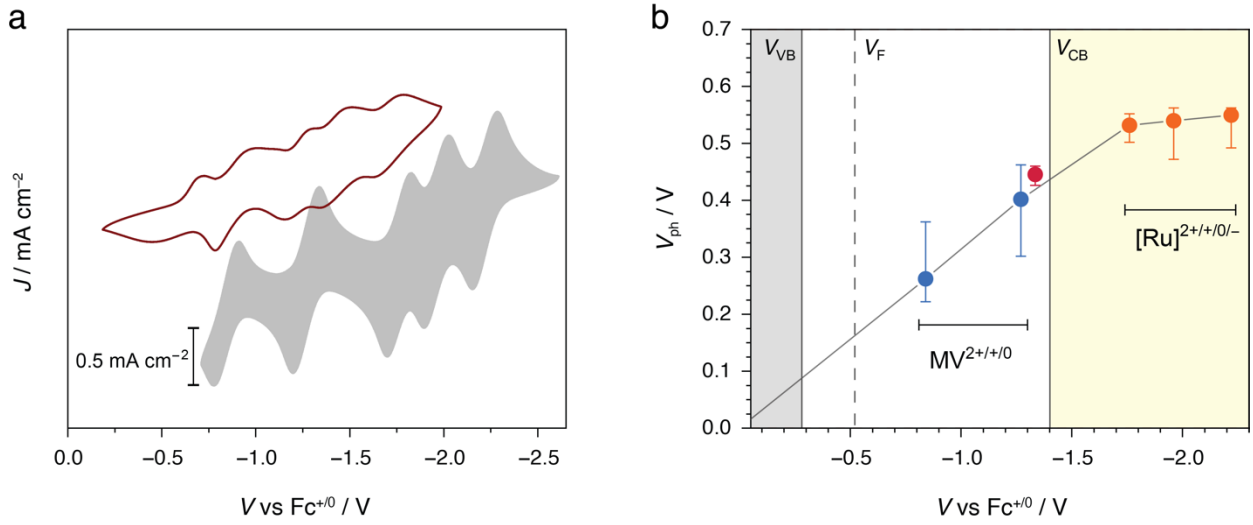

Figure 2. a) Cyclic voltammograms of MV^{2+} and $[Ru(bpy)_3]^{2+}$ (at 1 mM each) measured at 100 mV s^{-1} with a degenerately doped n^+-Si (gray scale) and p-Si(111) (red) illuminated with 34 mW/cm^2 of 650 nm light. b) Plot of the median photovoltages measured with the p-Si electrode for the indicated redox process versus the reduction potentials, with the minimum and maximum values indicated by the error bars. The *magenta* datapoint refers to measurements conducted with $CoCp_2$. Superimposed areas in gray and light yellow are the energetic positions of the p-Si valence and conduction bands at the estimated flat band condition.

Table 1. p-Si photovoltages and reduction potentials for the indicated redox couples.[a]

Redox Couple	V_{ph} / mV[a] (min, median, max)			$E°$ / V (n^+-Si)	E / V[a] (p-Si, median)
$MV^{2+/+}$	220	260	360	−0.84	−0.58
$MV^{+/0}$	300	400	460	−1.27	−0.87

$[Co(Cp)_2]^{+/0}$	433	440	441	−1.33	−0.89
$[Ru(bpy)_3]^{2+/+}$	500	530	550	−1.76	−1.23
$[Ru(bpy)_3]^{+/0}$	470	540	560	−1.96	−1.42
$[Ru(bpy)_3]^{0/-}$	490	550	560	−2.22	−1.67

[a]Reduction potentials are referenced versus the $Fc^{+/0}$ redox couple. Values for illuminated p-Si are statistical reports across 8 independent measurements.

Capacitance data were analyzed with a Mott-Schottky plot, i.e., $1/C^2$ *vs*. the applied potential, between –0.3 and –1.2 V vs $Fc^{+/0}$ with a step size of 10 mV. The capacitance, *C*, was extracted by modelling the impedance response of the photocathode with a single *RC* parallel circuit for frequencies greater than 300 Hz. Under these experimental conditions, the capacitance change was on the order of micro-Farads (expected for ideal space-charge layers in most semiconductors) and increased linearly with the applied voltage step between –0.4 and –0.7 V, with no evidence for significant Faradaic current.[36-37] The capacitance data were analyzed with Equation 1,

$$\frac{1}{C^2} = -\frac{2}{\varepsilon_0 \varepsilon_r e N_a A^2}\left(V - V_{fb} + \frac{kT}{e}\right) \qquad (1)$$

where, ε_0 is the dielectric permittivity of vacuum, $\varepsilon_r = 11.7$ is the dielectric permittivity of silicon, *e* is the elementary unit of charge, *A* is the geometric area of the photoelectrode in contact with the solution, *V* is the applied potential, *k* is the Boltzmann constant, and *T* is the absolute temperature. Representative Mott-Schottky plots measured from 300 Hz to 100 kHz are given in Figure S1 in a 0.1 M $TBAPF_6/CH_3CN$ with 1 mM each of MV^{2+} and $[Ru(bpy)_3]^{2+}$. The intercept provided an estimate of the flat band potential (V_{fb}) with an average value of –0.52 ±0.1 V vs $Fc^{+/0}$ that is in good agreement with previous literature reports for Si in acetonitrile electrolytes, for example V_{FB} = –0.43 V,[1] –0.61 V,[5] and –0.60 V,[49] all versus $Fc^{+/0}$. The slope provided an acceptor density (N_a ~ 10^{15} cm^{-3}) consistent with the value provided by the supplier. The valence and conduction band energies (V_{VB} = – 0.28 V vs $Fc^{+/0}$, and V_{VB} = – 1.4 V vs $Fc^{+/0}$) were determined as detailed in the Supporting Information. Capacitance measurements made in acetonitrile electrolyte with 10 mM concentrations of MV^{2+} or Rubpy resulted in the same flat band potentials as those measured in the neat electrolyte. The impact of including the reduced form(s) of the redox couples was not investigated herein.

Time-resolved infrared spectra measured at the indicated delay times after pulsed 532 nm excitation of p-Si are shown in Figure 3a. The spectra displayed as solid lines were measured in a dry N_2 ambient atmosphere, while the solid circles represent data measured at the open circuit condition in 0.1 M $TBAPF_6/CH_3CN$. Both the spectra and kinetics were largely insensitive to the

two environments. Strong absorption by the acetonitrile solvent near 3000 cm^{-1} and below 1600 cm^{-1} precluded measurements in these regions. The absorption increased with the wavelength raised to the second power, behavior consistent with the presence of free carriers (electrons and holes).[38] Spectroelectrochemical data *without bandgap excitation*, Figure 3b, also revealed the presence of free carriers when the applied potentials were poised at values more negative than V_{CB}. Stepping the potential back to potentials more positive than V_{CB} revealed that the spectral changes were reversible.

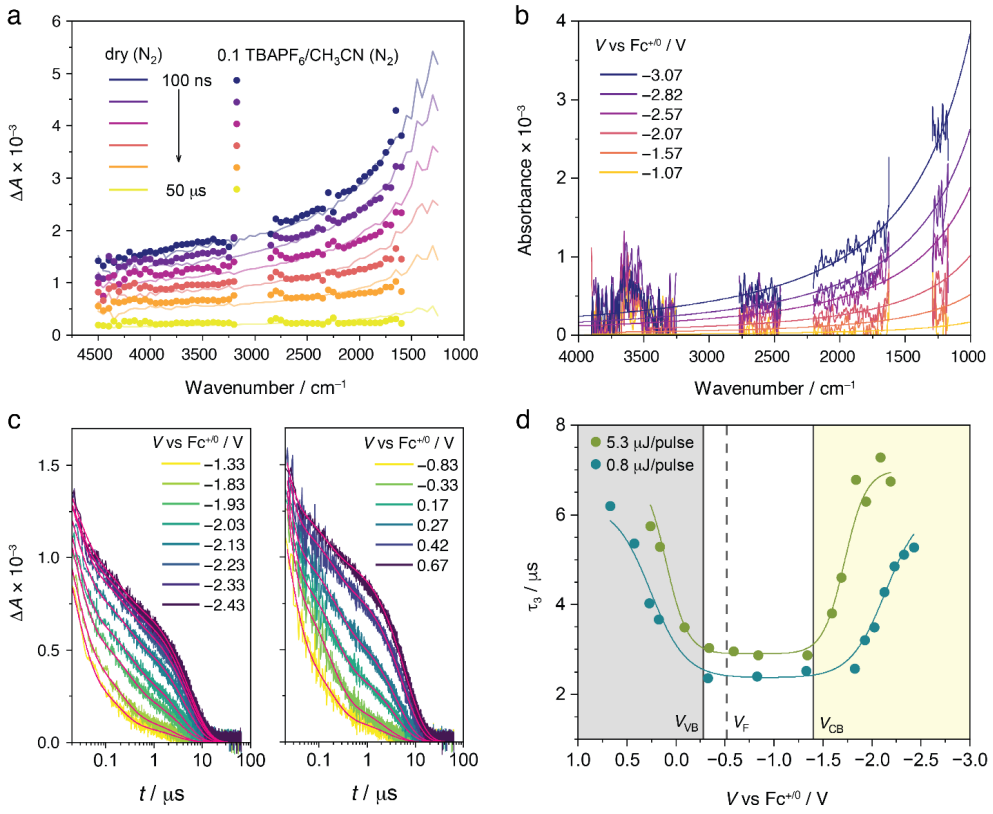

Figure 3. a) TRIR spectra measured 100 ns to 50 µs after pulsed 532 nm laser excitation of p-Si under N_2 (solid lines) and p-Si in 0.1 M $TBAPF_6/CH_3CN$ (circles). b) Spectroelectrochemical IR measurements of p-Si under increasingly negative applied potentials in the dark showing the free carrier generation entering inversion. c) Kinetic data monitored at 2000 cm^{-1} as a function of the applied potential with overlaid kinetic fits. d) Plot of τ_3, assigned to surface recombination, as a function of the applied potential for two light intensity conditions. The band edge positions at the flat band configuration are shown with solid interpolating curves to guide the eye.

The kinetic data were sensitive to the applied potential and light intensity yet were non-exponential under all conditions investigated. The data were fit to a sum of three exponentials (for details see Supporting Information). Kinetic data acquired as a function of the incident irradiance and the applied potential revealed that one of the three components ($\tau_3 = 1/k_3$) was highly sensitive

to both parameters while the other two components were not, Tables S1 and S2. The irradiance and applied potential dependent recombination pathway were hence assigned to surface recombination. We note that the term surface recombination velocity (cm/s) is often used to specify recombination at a surface.[30-31] Interestingly, kinetic data measured at applied potentials more negative than −1.0 V vs $Fc^{+/0}$ were far more sensitive to the light intensity than those measured at more positive applied potentials. Representative kinetic data measured at a fixed light intensity as a function of the applied potential are given in Figure 3c. Additional kinetic data measured with pulsed 410, 500, 600 and 700 nm laser excitation revealed no substantial differences in the recombination kinetics relative to 532 nm light.

Discussion

This study of multi-electron transfer at H-terminated p-Si acetonitrile electrolyte interfaces supports two important conclusions. First, the largest photovoltage values are realized when the molecular reduction potential coincides with the conduction band continuum of the semiconductor, not within the forbidden bandgap as is expected and predicted by Scheme 1. Second, all four electric field conditions known for a semiconductor junction in the solid state can also be accessed for semiconductor/electrolyte interfaces in photoelectrochemical cells. These findings are particularly encouraging for applications that require multi-electron transfer and specifically for the realization of liquid 'solar fuels' by CO_2 reduction with p-type hybrid semiconductor photoelectrodes.

These conclusions were garnered from electrochemical and spectroscopic measurements made as a function of the applied potential. Steady-state and time-resolved infrared spectroscopy were identified as particularly valuable experimental tools that distinguished inversion layer formation from Fermi-level pinning, a distinction that has historically been contentious in this field.[39] The bell-shaped dependence of the surface recombination rate with the applied potential predicted by a statistical model over 60 years ago was directly quantified through nanosecond transient infrared measurements. Next, we discuss the interfacial energetics measured in the dark, the impact of bandgap excitation, and the impact of these findings on multi-electron transfer catalysis within the context of the broader literature.

Interfacial Energetics. The approximate band edge positions of p-Si at the flat band condition were extracted from capacitance data while the formal reduction potentials were measured by cyclic voltammetry in a common electrolyte in the absence of bandgap illumination. These data indicate that the two MV^{2+} reductions (blue spheres) fall within the forbidden bandgap while the three $[Ru(bpy)_3]^{2+}$ potentials (orange spheres) are within the continuum of conduction band states, Figure 4a.

A literature review reveals that two different semiconductor/electrolyte potential distributions have been invoked to account for the saturation photovoltage behavior that arises from interfacial energetics like that reported here for $[Ru(bpy)_3]^{2+}$: 1) Inversion layer formation;[15, 33, 40-43] and 2) Fermi-level pinning (FLP)[23, 33, 39, 44-45]. In an inversion layer, the surface recombination rate is decreased as predicted by the SRH model.[15, 28, 32-33, 46] Under inversion conditions at high injection levels, the intrinsic Auger recombination rate may limit V_{ph} ,[47-49] but there is no experimental evidence to support this in the present study (vide infra). In Fermi-level pinning, intra-bandgap surface states exchange carriers with the bands that may unpin the band edges,[23, 39, 44-45] thereby limiting the magnitude of V_{ph} as is described in more detail below. We note that surface states present in an interfacial layer may also impact the magnitude of V_{oc} without giving rise to saturation behavior. For example, the presence of an dielectric layer, like SiO_2 on Si, may support a significant potential drop that results in a smaller V_{ph} value than expected.[50] Likewise, semiconductor functionalization with a material that possesses a large density of states, such as redox active monolayers,[6, 51-52] may yield a heterojunction with a smaller V_{ph} than that measured in the absence of the material. In the following discussion, focus is placed on inversion layer formation and FLP that give rise to the saturation photovoltage behavior reported herein.

Figure 4a provides a comparison of the potential distributions at a p-type semiconductor-electrolyte interface under ideal conditions with fixed band edge positions and in the presence of redox active surface states. As the Fermi level is raised from the flat band condition (reverse bias for a p-type semiconductor), a *depletion layer* is formed where the near surface region is depleted of majority carriers (holes for p-Si). When the Fermi level is raised further, to the point that it crosses the intrinsic Fermi level and is eventually poised above the conduction band edge at the interface, an inversion layer forms. The term *inversion* is used because, under these conditions, the type of majority carriers in the layer *inverts* to its opposite, e.g., electrons become dominant in a p-type semiconductor. Inversion layers are well known at solid-state interfaces such as in MOSFETs,[15, 32-33] but their formation at semiconductor-electrolyte interfaces in photoelectrochemical cells remains less certain.[45] Although less relevant to this study, lowering the Fermi-level from the flat band condition results in an accumulation layer, where majority carriers accumulate in the space charge region.

The potential distribution provided in Figure 4a were determined by solving the Poisson equation under the bias conditions of accumulation, flat band, and depletion were determined using the depletion approximationm, [15, 32-33] Equation 2 where $\rho(x)$ is the total charge density.

$$\frac{\mathrm{d}^2V(x)}{\mathrm{d}x^2} = -\frac{e}{\varepsilon_r\varepsilon_0}\rho(x) \qquad (2)$$

Positive values of x represent the bulk, with the surface fixed at $x = 0$. The conduction band potential at the surface remains fixed to its flat band value, $V_{CB}(0) = V_{CB}$, and at values of $x > 0$, $V_{CB}(x)$ shifts with the applied potential by an amount equivalent to the change in potential relative to flat band, $\Delta V = V_{app} - V_{fb}$. A similar boundary condition was applied to the valence band. Equation 2, with the appropriate approximation (depletion vs inversion) and boundary conditions, were solved in Mathematica, resulting in the typical parabolic band bending in the depletion layer.[16] Analytical solutions that more rigorously describe an inversion layer may be provided with additonal approximations that consider the effective density of states in the conduction and valence bands with utilization of the Fermi-Dirac distribution.[40-41]

The alternative case of semiconductor/electrolyte potential distribution occurs when a semiconductor has redox active surface states within the forbidden bandgap, Figure 4b. Under such conditions, raising the Fermi level from the flat band condition results in Faradaic electron transfer and partial reduction of the surface states. This redox chemistry pins the Fermi level and additional applied potential drops within the Helmholtz region of the electric double layer much like in a metal electrode. This condition is termed Fermi-level pinning (FLP). Historically, the observation of photovoltages that were insensitive to the formal reduction potential of a redox couple has been taken as direct evidence for FLP;[23, 39, 44-45, 53-54] however the data reported herein show that the same insensitivity is observed for an inversion layer. Hence additional data are neeeded to distinguish FLP from an inversion layer.

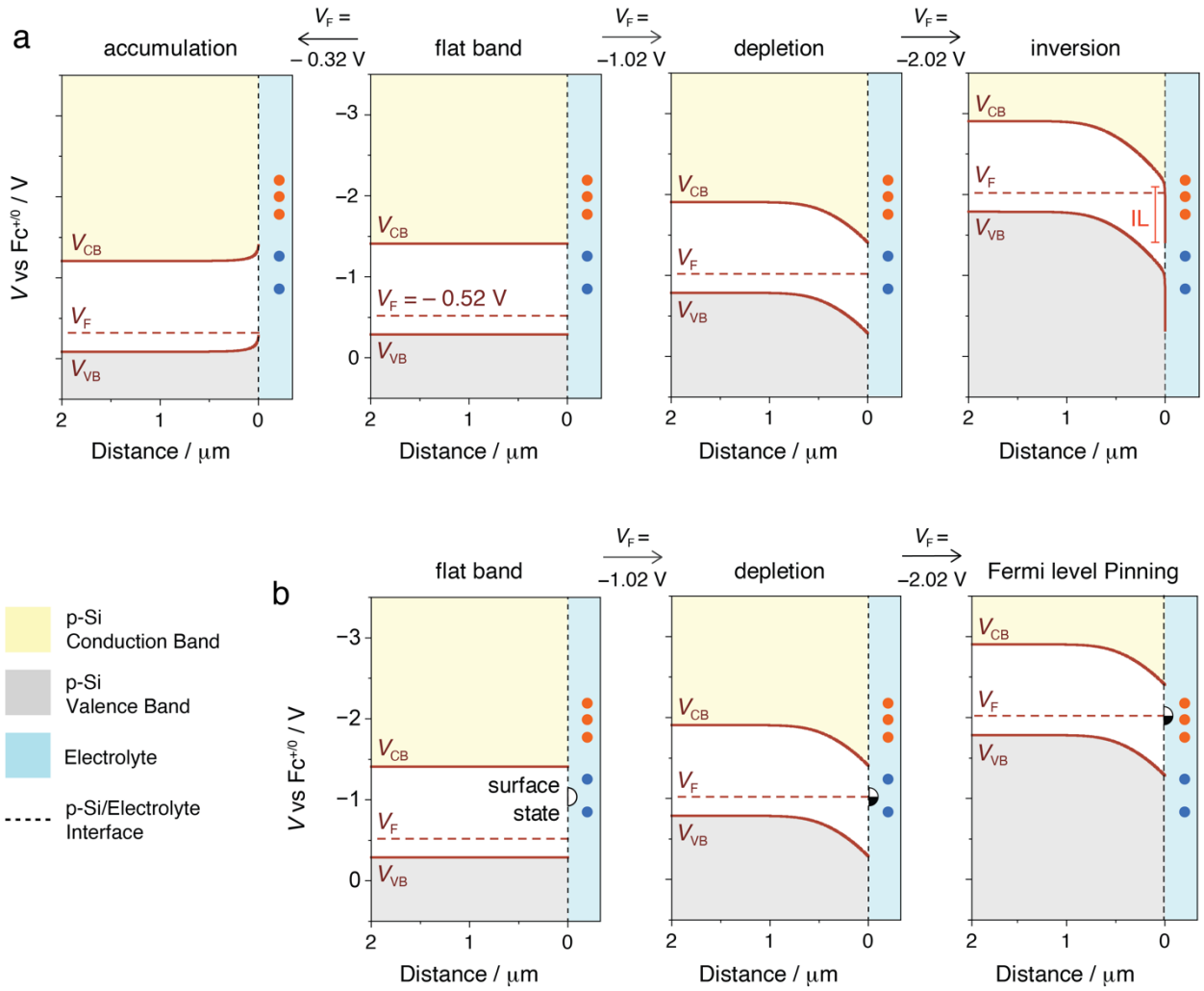

Figure 4. a) Band diagrams for an ideal surface with valence band (V_{VB}), Fermi level (V_F) and conduction band (V_{CB}) calculated as a function of the distance inside the semiconductor from the surface and applied potential for a H-terminated p-Si in contact with electrolyte without bandgap excitation. b) Fermi level equilibration with an applied potential for an interface with silicon surface states (represented by partially filled black semicircles) leading to Fermi level pinning. Reduction potentials for MV^{2+} (blue circles) and $[Ru(bpy)_3]^{2+}$ (orange circles) are included for comparison with the band diagrams.

A key distinguishing feature is the delocalized nature of conduction band electrons in an inversion layer, while a photoelectrode under FLP conditions has electrons present in localized surface states and a semiconductor under depletion conditions. For silicon, these surface states have historically been found at energies close to the intrinsic Fermi level.[15, 32-33] The spectroelectrochemical IR data reported here reveal the appearance of a long wavelength absorption as the Fermi level is raised to about –1.5 V vs $Fc^{+/0}$ that is lost when the potential is stepped back to more positive values. Free carrier absorption increases with wavelength raised to the second power, while trapped electrons in surface states are expected to show an absorption

maximum.[33, 38, 55-56] Therefore, the IR spectral data are most consistent with the presence of conduction band electrons in an inversion layer. Additional evidence for an inversion layer, as well as the other electric field conditions, was extracted from kinetic measurements made after bandgap excitation as described below.

Bandgap Excitation. It is worthwhile to consider Figure 4a with the assumption of isoenergetic electron transfer from fixed band edge positions. The first and second reductions of MV^{2+} by illuminated p-Si are expected and indeed observed as the potential for both redox couples lie within the forbidden bandgap. In contrast and contrary to experiment, the $[Ru(bpy)_3]^{2+}$ reductions lie within the continuum of conduction band states where efficient interfacial electron transfer is not expected based on Scheme 1.

Under depletion conditions, the electric field serves to separate charge, sweeping conduction band electrons toward the interface and valence band holes toward the bulk. Ideal photoelectrochemical behavior is well established in the literature under depletion conditions for a variety of semiconductors with ideal behavior often judged by plots of V_{ph} vs $E°(A^{0/-})$.[16, 22] The data reported here for the two viologen reductions are also fully consistent with depletion conditions and ideal behavior. The V_{ph} value for the second reduction, $MV^{+/0}$, is larger than the first, $MV^{2+/+}$, because the reduction potential is closer, but still below, the conduction band edge.[24] This energetic alignment leads to larger band bending in the dark, where it is hypothesized that larger electric fields reduce the concentration of holes at the surface, decreasing the effective rate of electron-hole pair recombination at the surface, therefore leading to a larger photovoltage.

Experimentally, the largest V_{ph} values were measured for $[Ru(bpy)_3]^{2+}$ that were, within experimental error, the same for all three redox couples. The consistent trend in the measured V_{ph} was: $MV^{2+/+}$ (260 mV) < $MV^{+/0}$ (400 mV) < $CoCp_2^{+/0}$ (450 mV) < $Ru^{2+/+}$ (530 mV) ~ $Ru^{+/0}$ (540 mV) ~ $Ru^{0/-}$ (550 mV). Historically, a constant photovoltage measured over a 440 mV range of $E°$ would be attributed to FLP. The larger photovoltage values would indicate surface states located energetically near V_{CB}. Indeed, by analogy to semiconductor-metal junctions that produce photovoltages insensitive to the metal work function, photoelectrochemists assigned FLP to semiconductor-electrolyte interfaces where the photovoltage was insensitive to $E°(A^{0/-})$. This analogy was described in three back-to-back papers published in *J. Am. Chem. Soc*.[23, 44, 57] However, negligibly small shifts in V_{ph} may also result when the quasi-Fermi level is raised further into inversion – as an inversion layer is formed, the band bending, and consequently the electric field, in the depletion region of the space charge layer saturates, and the excess potential drops in the Helmholtz planes of the electric double layer. Hence both FLP and inversion layer conditions may lead to V_{ph} values that are independent of $E°(A^{0/-})$. Both Gerischer and Nozik have previously suggested that behavior attributed to Fermi-level pinning could instead be a result of an inversion

layer.[42, 58] A Faraday Discussion on this topic noted that distinguishing FLP from an inversion layer was particularly problematic when the surface state energy was close to a band edge.[58]

The long wavelength absorption identified in spectroelectrochemical data is reasonably assigned to conduction band electrons and provides compelling evidence for the formation of an inversion layer when the applied potential is more negative than V_{CB}. These spectral data support previous evidence for inversion layer formation at semiconductor-electrolyte interfaces garnered through photo-capacitance and conductance measurements.[42-43]

Time-resolved infrared (TRIR) experiments following pulsed bandgap excitation provided additional evidence for this assignment and allowed the electron-hole pair lifetimes to be quantified. Historically, the recombination of photogenerated carriers has been quantified by time-resolved microwave conductivity measurements.[59-62] An advantage of the TRIR approach is that it enables *in situ* measurements in a photoelectrochemical cell as a function of the applied potential. When plotted as a rate contant, $k_3 = 1/\tau_3$, and normalized to the maximum value, $k_3/k_{3,max}$ a *bell-shaped* dependence on the applied potential results, Figure 5a. Stevenson and Keyes first reported a bell-shaped dependency of the surface recombination velocity on surface Fermi level position when the semiconductor interface accesses accumulation, flat band, depletion and inversion conditions with the applied potential consistent with what is now often called the Shockley-Read-Hall (SRH) recombination model.[15, 28, 32-33, 46] Such *bell-shaped* behavior is well documented for solid-state junctions,[29-30, 63] but to our knowledge has not been kinetically resolved in an operational photoelectrochemical cell.[31]

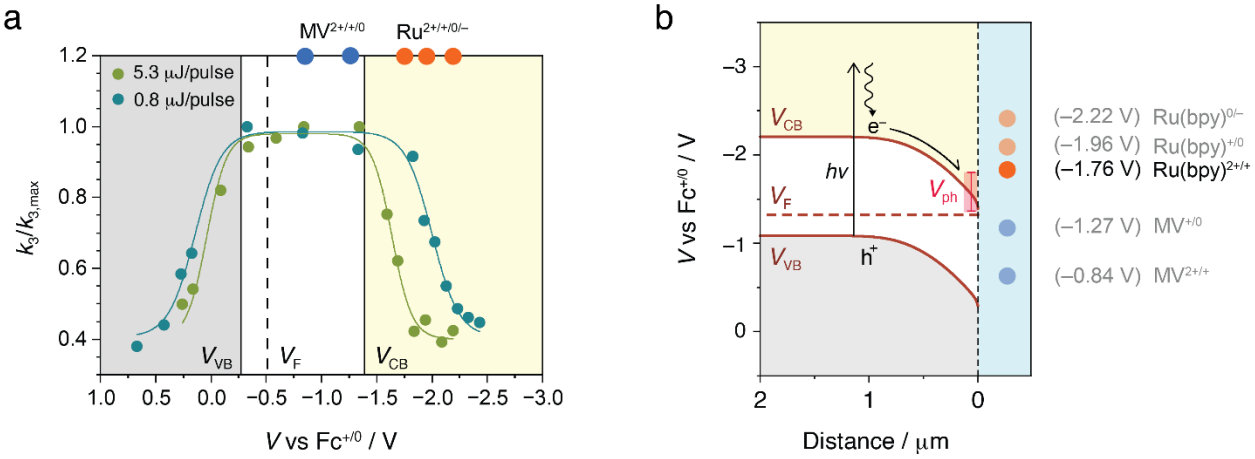

Figure 5. a) Plot of $k_3/k_{3,max}$ versus applied potential extracted from TRIR measurements as a function of the light intensity at low (0.8 μJ/pulse) and high (5.3 μJ/pulse) intensity. The positions of the band edges at the flat band condition are shown in the white area and the curves overlaying the experimental points are a guide to the eye. Reduction potentials for MV^{2+} (blue circles) and $[Ru(bpy)_3]^{2+}$ (orange circles) are included. b) Interfacial energetics at the p-Si electrolyte interface under illumination, taking the first reduction of $[Ru(bpy)_3]^{2+}$ as an example. The indicated

photovoltage, V_{ph} = 530 mV, corresponds to that measured by cyclic voltammetry in Figure 2a and Table 1.

In the SRH model, recombination is a maximum when the surface potential and electric field are not sufficiently strong to separate electrons and holes; this occurs at the flat band potential which is near the center of the *bell-shaped* curve.[32, 64-65] In contrast, electron-hole pair recombination is inhibited when an inversion layer is present as valence band holes are repelled from the surface and drift toward the bulk resulting in a depleted surface hole concentration. Indeed, the dramatically decreased recombination measured at positive and negative applied potentials are fully consistent with the presence of accumulation and inversion layers, respectively, and are not easily rationalized by other models.[28] If FLP were operative an increased lifetime would not be expected. Rather, the lifetime could decrease, due to carrier trapping by the surface states, or stay approximately the same as the applied potential falls in the electric double layer, without increased band bending; behavior that is contrary to what was measured experimentally.

Under inversion conditions the kinetic data were far more sensitive to the light intensity than that measured at potentials corresponding to flat band, depletion, or accumulation, Figure 5a. This behavior also has precedence in the solid-state literature where photogeneration of large numbers of conduction band electrons favors inversion layer formation.[32, 64-65] Indeed, the first reduction of may be very near the conduction band edge in the dark, with bandgap excitation resulting in inversion layer formation, Figure 5b. A redox couple with an E^o that coincides exactly with the conduction band edge in the dark would likely result in the same photovoltage as that measured in the conduction band continuum and may enter inversion when illuminated.

A switch from depletion conditions in the dark to an inversion in the light is important for photocatalysis and solar fuel applications. The onset of inversion occurs when the surface electron concentration is equal to the hole concentration in the bulk creating an n-type layer on a p-type semiconductor for enhanced charge separation. Strong inversion leads to conduction band electron concentrations of ~10^{20} cm^{-3}.[40-41] At such concentrations the semiconductor exhibits metal-like behavior and the applied potential falls in the electric double layer rather than in the semiconductor itself. This is expected to have a tremendous impact on the structure and composition of the electric double layer. For example, catalysts with large dipole moments would be expected to align with the electric field when illuminated with bandgap light,[66] while electrolyte cations would be electrostatically attracted to the hydrophobic H-terminated Si surface.[67] In future work, such behavior will be specifically examined with surface-sensitive attenuated total reflection infrared techniques and exploited to optimize catalysis with hybrid photoelectrodes.

The impact of these findings on prior photoelectrochemical research deserves some discussion. The photoelectrochemical behavior for H-terminated p-Si reported by Bocarsly and Wrighton and

attributed to FLP are likely instead due to inversion layer formation.[23-24, 44] Likewise, the large photovoltages and Faradaic yields reported in Kubiak's pioneering work on CO_2 photoreduction with Lehn's catalyst are also almost certainly due to the presence of an inversion layer.[1] The situation for III-V semiconductors and layered chalcogenide materials is less clear as a high density of surface states might be expected to underlie FLP behavior.[45, 68-69] However, as was first pointed out by Dare-Edwards, Bard's description of p-GaAs behaving as if it were coated with a monolayer of metal is more in line with behavior expected for an inversion layer than for electron transfer mediated by poorly defined surface states.[45,46] The data described herein establish the direct spectroelectrochemical detection of conduction band electrons as a general tool for distinguishing inversion from FLP.[61] Alternatively, *in situ* quantification of the surface recombination kinetics, accomplished herein by TRIR, as a function of the applied potential will certainly provide new insights. A decrease in the recombination rate is expected for an inversion layer and it will be of particular interest to test the assertion made herein that the surface recombination rate will increase or stay constant as the Fermi energy of a photoelectrode under FLP conditions is raised toward the vaccum level.

Conclusion

In summary, multi-electron transfer at H-terminated p-Si acetonitrile electrolyte interfaces revealed that the largest photovoltages are realized when the molecular reduction potential has the same energy level as the continuum of conduction band electrons. Steady state and time-resolved infrared spectroscopic measurements indicated that this behavior is due to the presence of an inversion layer, a surface layer where the dopant type has changed from p- to n-type. The inversion layer provides a high $\sim 10^{20}$ cm^{-3} surface electron concentration that supports multi-electron transfer with reduction potentials that span a 440 mV range. Therefore, the conundrum raised in the Introduction section and in Scheme 1 for optimizing multi-electron transfer, rather than a single transfer, is shown by experiment to be inconsequential. Indeed, the most ideal behavior was observed under inversion conditions with significantly smaller photovoltages generated when the reduction potential was within the forbidden bandgap. The photoelectrochemical behavior of the illuminated p-Si electrolyte interface under inversion conditions suggests an Ohmic-like semiconductor-molecule interface with the advantages of solar light harvesting to 1100 nm and metal-like behavior. The bell-shaped recombination kinetic data indicates that all four of the semiconductor electric field conditions known for solid state semiconductor junctions can also be accessed in photoelectrochemical cells. These behaviors are particularly encouraging for the realization of 'solar fuels' by multi-electron transfer catlaysis with hybrid semiconductor photoelectrodes.

Supporting Information for Publication.

Supporting Information material contains additional analysis of the Mott-Schottky and TRIR kinetic data.

Acknowledgement

This material is based upon work solely supported as part of the Center for Hybrid Approaches in Solar Energy to Liquid Fuels (CHASE), an Energy Innovation Hub funded by the U.S. Department of Energy, Office of Science, Office of Basic Energy Sciences under Award Number DE-SC0021173.

References

1. Kumar, B.; Smieja, J. M.; Kubiak, C. P., Photoreduction of CO_2 on p-type Silicon Using Re(bipy-But)$(CO)_3$Cl: Photovoltages Exceeding 600 mV for the Selective Reduction of CO_2 to CO. *The Journal of Physical Chemistry C* **2010,** *114* (33), 14220-14223.
2. Hou, Y.; Abrams, B. L.; Vesborg, P. C. K.; Björketun, M. E.; Herbst, K.; Bech, L.; Setti, A. M.; Damsgaard, C. D.; Pedersen, T.; Hansen, O.; Rossmeisl, J.; Dahl, S.; Nørskov, J. K.; Chorkendorff, I., Bioinspired Molecular Co-Catalysts Bonded to a Silicon Photocathode for Solar Hydrogen Evolution. *Nature Materials* **2011,** *10* (6), 434-438.
3. Gu, J.; Yan, Y.; Young, J. L.; Steirer, K. X.; Neale, N. R.; Turner, J. A., Water Reduction by a p-$GaInP_2$ Photoelectrode Stabilized by an Amorphous TiO_2 Coating and a Molecular Cobalt Catalyst. *Nature Materials* **2016,** *15* (4), 456-460.
4. Khusnutdinova, D.; Beiler, A. M.; Wadsworth, B. L.; Jacob, S. I.; Moore, G. F., Metalloporphyrin-Modified Semiconductors for Solar Fuel Production. *Chemical Science* **2017,** *8* (1), 253-259.
5. Gurrentz, J. M.; Rose, M. J., Non-Catalytic Benefits of Ni(II) Binding to an Si(111)-PNP Construct for Photoelectrochemical Hydrogen Evolution Reaction: Metal Ion Induced Flat Band Potential Modulation. *Journal of the American Chemical Society* **2020,** *142* (12), 5657-5667.
6. Hanna, C. M.; Pekarek, R. T.; Miller, E. M.; Yang, J. Y.; Neale, N. R., Decoupling Kinetics and Thermodynamics of Interfacial Catalysis at a Chemically Modified Black Silicon Semiconductor Photoelectrode. *ACS Energy Letters* **2020,** *5* (6), 1848-1855.
7. Wadsworth, B. L.; Nguyen, N. P.; Nishiori, D.; Beiler, A. M.; Moore, G. F., Addressing the Origin of Photocurrents and Fuel Production Activities in Catalyst-Modified Semiconductor Electrodes. *ACS Applied Energy Materials* **2020,** *3* (8), 7512-7519.
8. Laurans, M.; Wells, J. A. L.; Ott, S., Immobilising Molecular Ru Complexes on a Protective Ultrathin Oxide Layer of p-Si Electrodes Towards Photoelectrochemical CO_2 Reduction. *Dalton transactions* **2021,** *50* (30), 10482-10492.
9. Reyes Cruz, E. A.; Nishiori, D.; Wadsworth, B. L.; Nguyen, N. P.; Hensleigh, L. K.; Khusnutdinova, D.; Beiler, A. M.; Moore, G. F., Molecular-Modified Photocathodes for Applications in Artificial Photosynthesis and Solar-to-Fuel Technologies. *Chemical Reviews* **2022,** *122* (21), 16051-16109.
10. Wen, Z.; Xu, S.; Zhu, Y.; Liu, G.; Gao, H.; Sun, L.; Li, F., Aqueous CO_2 Reduction on Si Photocathodes Functionalized by Cobalt Molecular Catalysts/Carbon Nanotubes. *Angewandte Chemie International Edition* **2022,** *61* (24), e202201086.

11. Shang, B.; Rooney, C. L.; Gallagher, D. J.; Wang, B.; Krayev, A.; Shema, H.; Leitner, O.; Harmon, N. J.; Xiao, L.; Sheehan, C.; Bottum, S. R.; Gross, E.; Cahoon, J. F.; Mallouk, T. E.; Wang, H., Aqueous Photoelectrochemical CO2 Reduction to CO and Methanol over a Silicon Photocathode Functionalized with a Cobalt Phthalocyanine Molecular Catalyst. *Angewandte Chemie International Edition* **2022**.
12. Marcus, R. A., On the Theory of Electron-Transfer Reactions. VI. Unified Treatment for Homogeneous and Electrode Reactions. *The Journal of Chemical Physics* **1965,** *43* (2), 679-701.
13. Gerischer, H., Charge Transfer Processes at Semiconductor-Electrolyte Interfaces in Connection with Problems of Catalysis. *Surface Science* **1969,** *18* (1), 97-122.
14. Willig, F.; Gundlach, L., Redox Processes at Semiconductors-Gerischer Model and Beyond. In *Encyclopedia of Applied Electrochemistry*, Kreysa, G.; Ota, K.-i.; Savinell, R. F., Eds. Springer New York: New York, NY, 2014; pp 1786-1798.
15. Memming, R., *Semiconductor Electrochemistry*. Weinheim : Wiley-VCH, 2015.: Weinheim, 2015.
16. Gibbons, J. F.; Cogan, G. W.; Gronet, C. M.; Lewis, N. S., A 14% Efficient Nonaqueous Semiconductor/Liquid Junction Solar Cell. *Appl. Phys. Lett.* **1984,** *45* (10), 1095-1097.
17. Ross, R. T.; Nozik, A. J., Efficiency of Hot-Carrier Solar Energy Converters. *Journal of Applied Physics* **1982,** *53* (5), 3813-3818.
18. Cooper, G.; Turner, J. A.; Parkinson, B. A.; Nozik, A. J., Hot Carrier Injection of Photogenerated Electrons at Indium Phosphide-Electrolyte Interfaces. *Journal of Applied Physics* **1983,** *54* (11), 6463-6473.
19. Koval, C. A.; Segar, P. R., Mechanistic Aspects of Reductions by Hot Electrons in p-Indium Phosphide/Acetonitrile Photoelectrochemical Cells. *The Journal of Physical Chemistry* **1990,** *94* (5), 2033-2039.
20. Tisdale, W. A.; Williams, K. J.; Timp, B. A.; Norris, D. J.; Aydil, E. S.; Zhu, X.-Y., Hot-Electron Transfer from Semiconductor Nanocrystals. *Science* **2010,** *328* (5985), 1543-1547.
21. Zhang, C.; Fan, Y.; Huang, X.; Zhang, K. H. L.; Beard, M. C.; Yang, Y., Hot-Carrier Transfer at Photocatalytic Silicon/Platinum Interfaces. *The Journal of Chemical Physics* **2020,** *152* (14), 144705.
22. Lieber, C. M.; Gronet, C. M.; Lewis, N. S., Evidence Against Surface State Limitations on Efficiency of p-Si/CH_3CN Junctions. *Nature* **1984,** *307* (5951), 533-534.
23. Bocarsly, A. B.; Bookbinder, D. C.; Dominey, R. N.; Lewis, N. S.; Wrighton, M. S., Photoreduction at Illuminated p-type Semiconducting Silicon Photoelectrodes. Evidence for Fermi Level Pinning. *Journal of the American Chemical Society* **1980,** *102* (11), 3683-3688.
24. Wrighton, M. S., Photoelectrochemical Conversion of Optical Energy to Electricity and Fuels. *Accounts of Chemical Research* **1979,** *12* (9), 303-310.
25. Yablonovitch, E.; Allara, D. L.; Chang, C. C.; Gmitter, T.; Bright, T. B., Unusually Low Surface-Recombination Velocity on Silicon and Germanium Surfaces. *Physical Review Letters* **1986,** *57* (2), 249-252.
26. Higashi, G. S.; Chabal, Y. J.; Trucks, G. W.; Raghavachari, K., Ideal Hydrogen Termination of the Si (111) Surface. *Appl. Phys. Lett.* **1990,** *56* (7), 656-658.
27. Dumas, P.; Chabal, Y. J.; Jakob, P., Morphology of Hydrogen-Terminated Si(111) and Si(100) Surfaces Upon Etching in HF and Buffered-HF Solutions. *Surface Science* **1992,** *269-270*, 867-878.
28. Stevenson, D. T.; Keyes, R. J., Measurements of the Recombination Velocity at Germanium Surfaces. *Physica* **1954,** *20* (7), 1041-1046.

29. Dousmanis, G. C., Semiconductor Surface Potential and Surface States from Field-Induced Changes in Surface Recombination. *Physical Review* **1958,** *112* (2), 369-380.
30. Dousmanis, G. C., Effects of Carrier Injection on the Recombination Velocity in Semiconductor Surfaces. *Journal of Applied Physics* **1959,** *30* (2), 180-184.
31. Memming, R., Surface Recombination at Higher Injection Levels. *Surface Science* **1964,** *1* (1), 88-101.
32. Many, A.; Goldstein, Y.; Grover, N. B., *Semiconductor Surfaces*. Amsterdam, North-Holland Pub. Co.; New York, Interscience Publishers, 1965.: Amsterdam, 1965.
33. Sze, S. M.; Ng, K. K., *Physics of Semiconductor Devices*. Hoboken, N.J. : Wiley-Interscience.: Hoboken, N.J., 2007.
34. Grills, D. C.; Farrington, J. A.; Layne, B. H.; Preses, J. M.; Bernstein, H. J.; Wishart, J. F., Development of Nanosecond Time-Resolved Infrared Detection at the LEAF Pulse Radiolysis Facility. *Review of Scientific Instruments* **2015,** *86* (4), 044102.
35. Sampaio, R. N.; Grills, D. C.; Polyansky, D. E.; Szalda, D. J.; Fujita, E., Unexpected Roles of Triethanolamine in the Photochemical Reduction of CO_2 to Formate by Ruthenium Complexes. *Journal of the American Chemical Society* **2020,** *142* (5), 2413-2428.
36. Hankin, A.; Bedoya-Lora, F. E.; Alexander, J. C.; Regoutz, A.; Kelsall, G. H., Flat-Band Potential Determination: Avoiding the Pitfalls. *Journal of Materials Chemistry A* **2019,** *7* (45), 26162-26176.
37. Sivula, K., Mott–Schottky Analysis of Photoelectrodes: Sanity Checks Are Needed. *ACS Energy Letters* **2021,** *6* (7), 2549-2551.
38. Schroder, D. K.; Thomas, R. N.; Swartz, J. C., Free Carrier Absorption in Silicon. *IEEE Journal of Solid-State Circuits* **1978,** *13* (1), 180-187.
39. Lewerenz, H. J., Surface States and Fermi level Pinning at Semiconductor/Electrolyte Junctions. *Journal of Electroanalytical Chemistry* **1993,** *356* (1), 121-143.
40. Hauser, J. R.; Littlejohn, M. A., Approximations for Accumulation and Inversion Space-Charge Layers in Semiconductors. *Solid-State Electronics* **1968,** *11* (7), 667-674.
41. Demoulin, E.; van de Wiele, F., Inversion Layer at the Interface of Schottky Diodes. *Solid-State Electronics* **1974,** *17* (8), 825-833.
42. Turner, J. A.; Manassen, J.; Nozik, A. J., Photoelectrochemistry with p-Si Electrodes: Effects of Inversion. *Appl. Phys. Lett.* **1980,** *37* (5), 488-491.
43. Lewis, N. S., A Quantitative Investigation of the Open-Circuit Photovoltage at the Semiconductor/Liquid Interface. *Journal of The Electrochemical Society* **1984,** *131* (11), 2496-2503.
44. Bard, A. J.; Bocarsly, A. B.; Fan, F. R. F.; Walton, E. G.; Wrighton, M. S., The Concept of Fermi Level Pinning at Semiconductor/Liquid Junctions. Consequences for Energy Conversion Efficiency and Selection of Useful Solution Redox Couples in Solar Devices. *Journal of the American Chemical Society* **1980,** *102* (11), 3671-3677.
45. Bard, A. J.; Fan, F.-R. F.; Gioda, A. S.; Nagasubramanian, G.; White, H. S., On the Role of Surface States in Semiconductor Electrode Photoelectrochemical Cells. *Faraday Discussions of the Chemical Society* **1980,** *70* (0), 19-31.
46. Michalak, D. J.; Gstrein, F.; Lewis, N. S., The Role of Band Bending in Affecting the Surface Recombination Velocities for Si(111) in Contact with Aqueous Acidic Electrolytes. *The Journal of Physical Chemistry C* **2008,** *112* (15), 5911-5921.
47. Sinton, R. A.; Swanson, R. M., Recombination in Highly Injected Silicon. *IEEE Trans. Electron Devices* **1987,** *34* (6), 1380-1389.

48. Hangleiter, A.; Häcker, R., Enhancement of Band-to-Band Auger Recombination by Electron-Hole Correlations. *Physical Review Letters* **1990,** *65* (2), 215-218.
49. Schroder, D. K., Carrier Lifetimes in Silicon. *IEEE Trans. Electron Devices* **1997,** *44*, 160-170.
50. Singh, R.; Green, M. A.; Rajkanan, K., Review of conductor-insulator-semiconductor (CIS) solar cells. *Solar Cells* **1981,** *3* (2), 95-148.
51. Eggers, P. K.; Darwish, N.; Paddon-Row, M. N.; Gooding, J. J., Surface-Bound Molecular Rulers for Probing the Electrical Double Layer. *Journal of the American Chemical Society* **2012,** *134* (17), 7539-7544.
52. Bhowmick, D. K.; Urban, A. J.; Bartsch, M.; Braunschweig, B.; Zacharias, H., Near-UV-Induced Rapid Formation of Compact Self-Assembled Organophosphonate Monolayers on H-Terminated Si(111) Surfaces. *The Journal of Physical Chemistry C* **2022**.
53. Grimm, R. L.; Bierman, M. J.; O'Leary, L. E.; Strandwitz, N. C.; Brunschwig, B. S.; Lewis, N. S., Comparison of the Photoelectrochemical Behavior of H-Terminated and Methyl-Terminated Si(111) Surfaces in Contact with a Series of One-Electron, Outer-Sphere Redox Couples in CH3CN. *The Journal of Physical Chemistry C* **2012,** *116* (44), 23569-23576.
54. Kearney, K. L.; Rockett, A. A., Simulation of Charge Transport and Recombination across Functionalized Si(111) Photoelectrodes. *Journal of The Electrochemical Society* **2016,** *163* (7), H598.
55. Reed, A. H.; Yeager, E., Infra-Red Internal Reflexion Studies of the Germanium/Electrolyte Interface. *Electrochimica Acta* **1970,** *15* (8), 1345-1354.
56. Harrick, N. J., Optical Spectrum of the Semiconductor Surface States from Frustrated Total Internal Reflections. *Physical Review* **1962,** *125* (4), 1165-1170.
57. Fan, F. R. F.; Bard, A. J., Semiconductor Electrodes. 24. Behavior of Photoelectrochemical Cells Based on p-type Gallium Arsenide in Aqueous Solutions. *Journal of the American Chemical Society* **1980,** *102* (11), 3677-3683.
58. Dare-Edwards, M. P.; Bard, A. J.; Faulkner, L. R.; Bockris, J. O. M.; Khan, S. U. M.; Uosaki, K.; Gerischer, H.; Nozik, A. J.; Schumacher, R.; Ellis, A. B.; Harzion, Z.; Albery, W. J.; Davidson, R. S.; Perone, S. P.; Richardson, J. H.; Archer, M. D.; Gissler, W.; Pichat, P.; Ginley, D. S.; Jarrett, H. S.; Butler, M. A.; Armstrong, N.; Gomes, W. P.; Peter, L. M.; Froelicher, M.; Malati, M. A.; Lemasson, P.; Potter, R.; Hamnett, A.; Sprünken, H. R., General Discussion. *Faraday Discussions of the Chemical Society* **1980,** *70* (0), 93-132.
59. Forbes, M. D. E.; Lewis, N. S., Real-Time Measurements of Interfacial Charge Transfer Rates at Silicon/Liquid Junctions. *Journal of the American Chemical Society* **1990,** *112* (9), 3682-3683.
60. Swiatkowski, C.; Sanders, A.; Buhre, K. D.; Kunst, M., Charge-Carrier Kinetics in Semiconductors by Microwave Conductivity Measurements. *Journal of Applied Physics* **1995,** *78* (3), 1763-1775.
61. Vasquez, R. M.; Hlynchuk, S.; Maldonado, S., Effect of Covalent Surface Functionalization of Si on the Activity of Trifluoromethanesulfonic Anhydride for Suppressing Surface Recombination. *ACS Applied Materials & Interfaces* **2020,** *12* (51), 57560-57568.
62. Boucher, D. G.; Kearney, K.; Ertekin, E.; Rose, M. J., Tuning p-Si(111) Photovoltage via Molecule|Semiconductor Electronic Coupling. *Journal of the American Chemical Society* **2021,** *143* (6), 2567-2580.

63. Adamowicz, B.; Hasegawa, H., Computer Analysis of Surface Recombination Process at Si and Compound Semiconductor Surfaces and Behavior of Surface Recombination Velocity. *Japanese Journal of Applied Physics* **1998,** *37* (3S), 1631.
64. Nedeljkovic, M.; Soref, R.; Mashanovich, G. Z., Free-Carrier Electrorefraction and Electroabsorption Modulation Predictions for Silicon Over the 1–14 μm Infrared Wavelength Range. *IEEE Photonics Journal* **2011,** *3* (6), 1171-1180.
65. Iqbal, A.; Bevan, K. H., The Impact of Boundary Conditions on Calculated Photovoltages and Photocurrents at Photocatalytic Interfaces. *MRS Communications* **2018,** *8* (2), 466-473.
66. Sampaio, R. N.; Li, G.; Meyer, G. J., Flipping Molecules Over on TiO_2 Surfaces with Light and Electric Fields. *Journal of the American Chemical Society* **2019,** *141* (35), 13898-13904.
67. Rao, A. V.; Chazalviel, J. N.; Ozanam, F., In situ Characterization of the n-Si/acetonitrile Interface by Electromodulated Infrared Internal-Reflection Spectroscopy. *Journal of Applied Physics* **1986,** *60* (2), 696-706.
68. Fan, F.-R. F.; White, H. S.; Wheeler, B. L.; Bard, A. J., Semiconductor Electrodes. 31. Photoelectrochemistry and Photovoltaic Systems with n- and p-type Tungsten Selenide (WSe_2) in Aqueous Solution. *Journal of the American Chemical Society* **1980,** *102* (16), 5142-5148.
69. White, H. S.; Fan, F. R. F.; Bard, A. J., Semiconductor Electrodes: XXXIII . Photoelectrochemistry of n-Type in Acetonitrile. *Journal of The Electrochemical Society* **1981,** *128* (5), 1045.

TOC Graphics

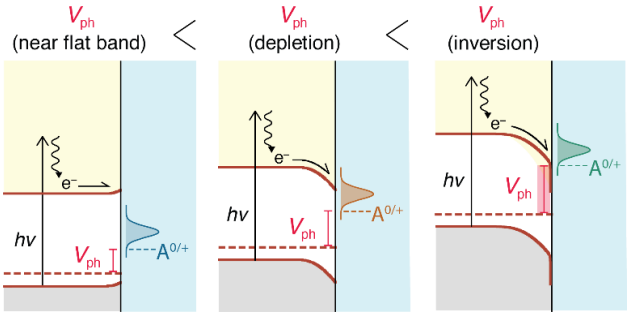

SUPPORTING INFORMATION

Multi-Electron Transfer at H-terminated p-Si Electrolyte Interfaces: Large Photovoltages under Inversion Conditions

Niklas D. Keller,[1] Pierpaolo Vecchi,[1,2] David C. Grills,[3] Dmitry E. Polyansky,[3] Gabriella P. Bein,[1] Jillian L. Dempsey,[1] James F. Cahoon,[1] Gregory N. Parsons,[4] Renato N. Sampaio,[1]* and Gerald J. Meyer[1]*

[1]Department of Chemistry, University of North Carolina at Chapel Hill, Chapel Hill, NC 27599
[2]Department of Physics and Astronomy, University of Bologna, Bologna, Italy 40127
[3]Chemistry Division, Brookhaven National Laboratory, Upton, NY 11973-5000
[4]Department of Chemical and Biomolecular Engineering, North Carolina State University, Raleigh, North Carolina 27695-7905

TABLE OF CONTENTS

1 Analysis of Mott-Schottky Data and Flat-Band Energy Diagram

The slope obtained from the linear fit of the Mott-Schottky plot (Figure below) was used to calculate the acceptor density (N_a) according to equation S1,

$$N_a = \frac{2}{e\,A^2\,\varepsilon_r\,\varepsilon_0 \times slope} \qquad \text{eq. S1}$$

where e is the elementary charge, A is the area of the electrode in contact with the electrolyte, ε_r is the relative permittivity of Si ($\varepsilon_r = 11.7$), and ε_0 is the vacuum permittivity, ε_0.

The energetic position of the Fermi level (E_F), relative to the intrinsic Fermi energy ($E_{F,i}$), was obtained according to equation S2,

$$V - V_F = \ln\left(\frac{n_i}{N_a}\right) \times kT \qquad \text{eq. S2}$$

where n_i is the intrinsic carrier density of silicon (1.5×10^{10} cm^{-3}), kT = 0.0259 eV at room temperature, $V_{F,i}$ is the intrinsic Fermi level, and the Fermi level V_F is equal to V_{fb}.

The positions of the conduction (V_{CB}) and valence (V_{VB}) band edges were determined using the relations $V_{VB} = V_{F,i} + V_{bg}/2$, and $V_{CB} = V_{F,i} - V_{bg}/2$. V_{bg} is equal to the voltage difference between the valence and conduction band edges (1.12 V), which is related to the bandgap energy of silicon (1.12 eV).

The average flatband potential of −0.52 (±0.1) V vs $Fc^{+/0}$ was determined by Mott-Schottky analysis on 12 different silicon electrodes in the dark at frequencies from 300 Hz to 100 kHz. The dopant concentration, N_a was in the range from 7.34×10^{14} cm^{-3} to 1.52×10^{16} cm^{-3}, which matches the supplier's information of (1 – 20 Ω cm → 1.49×10^{14} cm^{-3} to 6.64×10^{16} cm^{-3}). The average difference of $V_{fb} - V_{VB}$ was determined to be 0.24 (±0.04) eV.

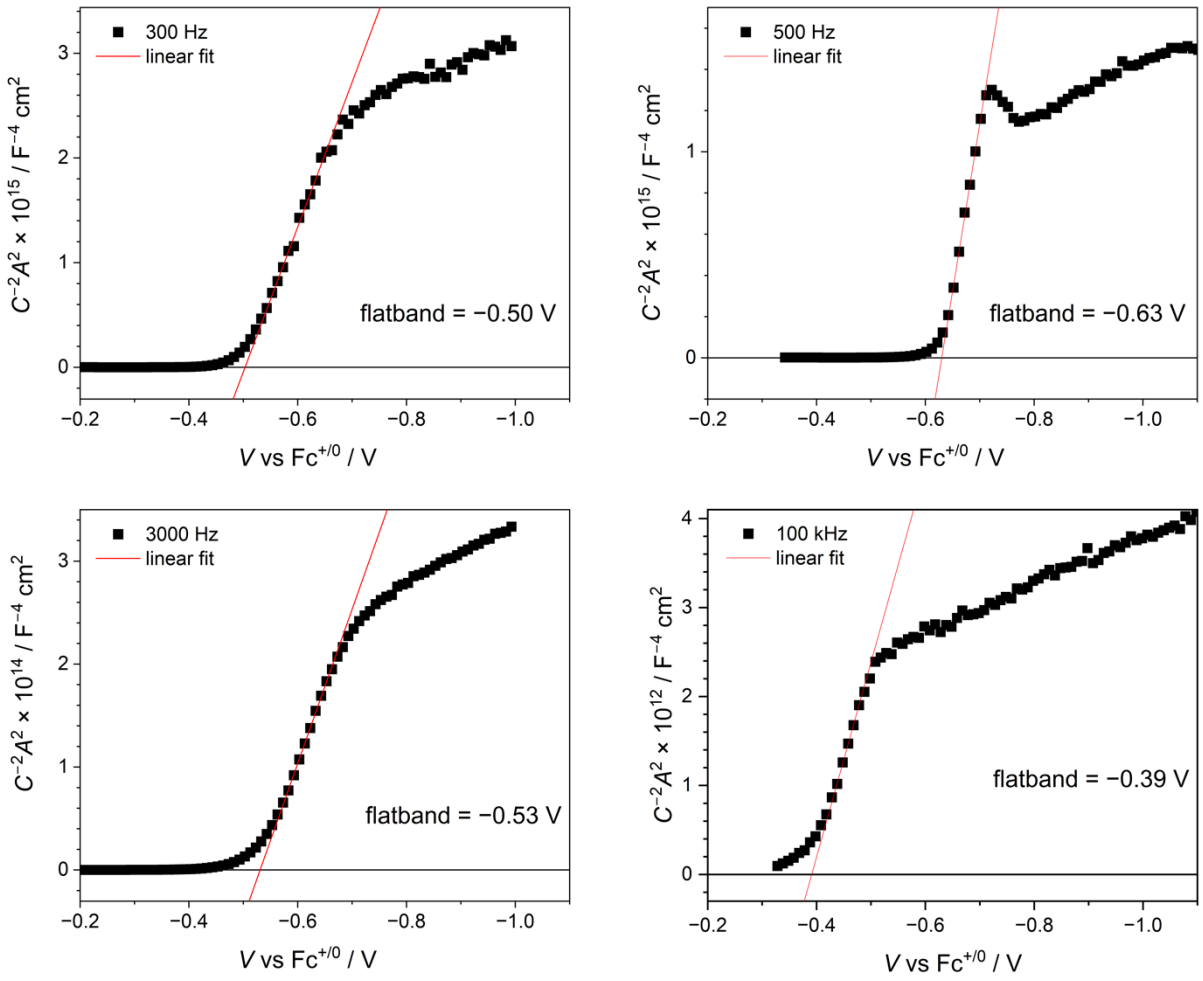

Figure S1: Selected Mott-Schottky analyses of p-Si in electrolyte (0.1 M $TBAPF_6/CH_3CN$) containing $[Ru(bpy)_3]^{2+}$ and MV^{2+} (1 mM). The measurements were taken in the dark at the indicated frequencies from 300 Hz to 100 kHz. The flatband potentials, determined by the intersect of the linear fit and the x-axis, are given in each plot.

2 Analysis of the TRIR Kinetic Data

The kinetic data obtained from TRIR measurements were analyzed with a tri-exponential kinetic model, equation S3.

$$\Delta A(t) = A_1(\exp -t/\tau_1) + A_2(\exp -t/\tau_2) + A_3(\exp -t/\tau_3) \qquad \text{eq. S3}$$

Best-fits to data acquired after pulsed 532 nm excitation at 5.3 μJ/pulse and 0.8 μJ/pulse as a function of the applied potential are given in Tables S1 and S2, respectively. Both τ_1 and τ_2 were nearly insensitive to the applied voltage and the incident irradiance, while τ_3 was markedly sensitive to both. The assignment of the slow component, τ_3, to surface recombination was made

based on this observation; the other kinetic contributions (τ_1 and τ_2) likely result from carrier recombination in the bulk of the material. It should be noted that the use of an 'average' rate constant, based on the weighted average of the three components, yields the same bell-shaped dependence on the applied potential shown in Figure 4 and does not impact the conclusions in this paper.

Table S1: Free-carrier lifetimes in p-Si measured after pulsed 532 nm excitation at 0.8 μJ/pulse.[a]

Potential	τ_1	A_1	τ_2	A_2	τ_3	A_3
V vs $Fc^{+/0}$	ns	%	ns	%	μs	%
−1.33	18	76	151	18	2.49	6
−1.83	20	70	189	21	2.57	9
−1.93	24	62	263	21	3.23	17
−2.03	20	59	247	18	3.49	23
−2.13	18	55	211	16	4.28	29
−2.23	15	55	197	14	4.85	31
−2.33	12	60	170	12	5.10	28
−2.43	12	60	154	12	5.26	28

[a]The electrolyte was 0.1 M $TBAPF_6/CH_3CN$ and the lifetimes were extracted from a tri-exponential fit of kinetic data monitored at 2000 cm^{-1}. Errors of 1-10% to the extracted lifetimes represent uncertainties from the fit.

Table S2: Free-carrier lifetimes in p-Si measured after pulsed 532 nm excitation at 5.3 μJ/pulse.[a]

Potential	τ_1	A_1	τ_2	A_2	τ_3	A_3
V vs $Fc^{+/0}$	ns	%	ns	%	μs	%
−1.34	19	79	208	16	2.94	5
−1.59	19	77	233	15	3.80	8
−1.69	21	74	251	16	4.60	10
−1.84	19	72	259	14	6.77	14
−1.94	21	70	267	16	6.29	14
−2.09	19	70	265	15	7.28	15
−2.19	20	71	260	15	6.75	14

[a]The electrolyte was 0.1 M $TBAPF_6/CH_3CN$ and the lifetimes were extracted from a tri-exponential fit of kinetic data monitored at 2000 cm^{-1}. Errors of 1-10% to the extracted lifetimes represent uncertainties from the fit.